



# Forensic analysis methodology for thermal and chemical characterization of homemade explosives



Ashot Nazarian, Cary Presser\*

National Institute of Standards and Technology, United States

## ARTICLE INFO

### Article history:

Received 3 June 2013

Received in revised form 8 August 2013

Accepted 31 October 2013

Available online 24 November 2013

### Keywords:

Ammonium nitrate

Homemade explosives

Forensic analysis

Laser-driven thermal reactor

Nitromethane

Thermal/chemical signatures

## ABSTRACT

Forensic identification of homemade explosives is critical for determining the origin of the explosive materials and precursors, and formulation procedures. Normally, the forensic examination of the pre- and post-blast physical evidence lacks specificity for homemade-explosive identification. The focus of this investigation was to use a novel measurement technique, referred to as the laser-driven thermal reactor, to obtain the thermal/chemical signatures of homemade-explosive precursor materials. Specifically, nitromethane and ammonium nitrate were studied under a variety of operating conditions and protocols. Results indicated that liquid-fuel saturation of the internal pores of a solid particle oxidizer appear to be a limiting parameter for the total specific heat release during exothermic processes. Results also indicated that the thermal signatures of these materials are dependent on sample mass and heating rate, for which this dependency may not be detectable by other commercially available thermal analysis techniques. This study has demonstrated that the laser-driven thermal reactor can be a useful diagnostic tool for characterizing the thermal and chemical behavior of trace amounts of homemade-explosive materials.

Published by Elsevier B.V.

## 1. Introduction

### 1.1. Background and forensic needs

Homemade explosives (HME) (i.e., the synthesized chemical product that is derived from precursor materials) are being used increasingly by extremists and terrorists due to the widespread availability and easy accessibility of the precursors. This is a major concern expressed by the Federal Government [1] with regard to improvised explosive devices of which HMEs are an essential component. Accurate forensic information on HMEs is critical for (a) identifying the origin of the explosive materials and precursors, and (b) determining HME formulation and synthesis procedures. The forensic examination of the pre- and post-blast physical evidence lacks specificity for HME identification. Development of a thermal-/chemical-signature database, obtained for pre-selected HME precursor materials, would assist in forensic processing and analysis of data recovered from HME target locations (i.e., pre- and post-blast sites). A database would reduce HME identification uncertainty (e.g., mixture composition, preparation history, possible precursor sources) and forensic processing time. The availability

of accurate HME data can be also used by the forensic science community to help law enforcement and military agencies disrupt or discourage the manufacture of HME chemical formulations, and provide protocols for safe HME disposal.

According to the Department of Defense [2], there is a need to improve forensic capabilities by developing new (a) measurement techniques to identify HME chemical and physical signatures, as well as observables characteristics, (b) methodologies to identify HME precursor sources, as well as their formation and handling protocols, and (c) tools to identify the initial chemical components from post-blast residue compositions. Two of the more commonly used HME materials are ammonium nitrate and nitromethane. The thermal behavior of ammonium nitrate (AN) is important from both industry and national security perspectives. In agriculture, ammonium nitrate is used mainly as a nitrogen fertilizer. There is also an industrial use for ammonium nitrate as an explosive material [3]. As a national security issue, extremists commonly use AN to manufacture homemade explosives.

### 1.2. Thermal analysis methodologies

Thermal analysis methodologies are commonly used to analyze the thermal changes of a sample due to heating and cooling. The sample characteristics that are derived from thermal analysis techniques include thermal (e.g., temperature, heat, enthalpy), physical (e.g., mass, volume, strength), and chemical (e.g., chemical

\* Corresponding author at: National Institute of Standards and Technology, Bldg. 221, Rm. B310, 100 Bureau Dr., Stop 8320, Gaithersburg, MD 20899-8320, United States. Tel.: +1 301 975 2612.

E-mail address: [cpresser@nist.gov](mailto:cpresser@nist.gov) (C. Presser).

**Nomenclature**

$A$	sample geometric cross-sectional area [ $\text{m}^2$ ]
$c_p(T)$	specific heat capacity [ $\text{J g}^{-1} \text{K}^{-1}$ ]
$(dT/dt)$	sample temperature–time derivatives [ $\text{K s}^{-1}$ ]
$F(T, T_0)$	heat transfer term [W]
$I_l$	intensity of the laser beam that heats the sample [ $\text{W m}^{-2}$ ]
$k$	coverage factor
$m(t)$	sample total initial mass [g]
$n$	number of samples
$q(T)$	specific heat release rate due to chemical reaction [ $\text{W g}^{-1}$ ]
$Q$	total specific heat release (or absorption) [ $\text{kJ g}^{-1}$ ]
$R_{lh}$	laser heating rate [ $\text{K s}^{-1}$ ]
$R_1(T_r)$	rate at which thermal energy is transferred from the reactor to the sample [W]
$R_2(T)$	rate of thermal energy loss from the sample and substrate [W]
$s$	standard deviation
$t$	time [s]
$T$	temperature [K]
$T_a$	ambient temperature [K]
$T_o$	steady-state sample temperature [K]
$T_r$	reactor temperature [K]
$T_1, T_2$	sample temperatures at different laser fluences [K]
$u_c$	combined uncertainty
$y, y_o$	nitromethane/activated carbon mass ratio, initial value

*Greek symbols*

$\beta(T)$	absorptivity
$\lambda$	laser wavelength [m]
$\Delta H$	change in enthalpy [ $\text{kJ g}^{-1}$ ]
$\Delta m$	mass for the reactive portion of the sample [g]
$\Delta T$	change in temperature [K]
$\Delta t$	change in time [s]
$\tau(T)$	temperature-dependent relaxation time [s]

*Subscripts*

$sa$	sample and substrate
$so$	substrate only

composition of products) characteristics. There are a variety of commercially available measurement techniques that have been developed and used to meet these needs. Thermal analysis techniques, such as differential scanning calorimetry (DSC) and thermal gravimetric analysis (TGA) are commonly employed in research to provide information on the material explosive/energetic content and other thermal properties (e.g., decomposition, heating value, and thermal stability), and also for composition identification of an unknown explosive material.

Vyazovkin et al. [4] investigated the gasification kinetics of both solid and liquid AN, and provided the chemical kinetics. The thermal dissociation of solid and liquid AN was analyzed using DSC/TGA methods. The experimental measurements were carried out at low heating rates between 2.5 and 12.5 °C min<sup>-1</sup>. The resulting chemical kinetics mechanism was assigned to the process of dissociative sublimation/vaporization. Oxley et al. [5] carried out an investigation using DSC to explore if this technique could be used as a benchmark for evaluating the explosivity of ammonium nitrate. In this study, thermal analysis was used to screen a large number of AN formulations in search of possible deterrents. They found that sodium, potassium, ammonium and calcium salts of

sulfate, phosphate, or carbonate, as well as certain high-nitrogen organics, can enhance AN thermal stability. The need to improve thermal analysis techniques was also emphasized by Desilets et al. [6]. In this work, the thermal decomposition of urea nitrate (UN) was studied at higher temperatures. The UN non-isothermal decomposition kinetics and products of reaction were analyzed using a DSC/TGA instrument in conjunction with Fourier transform infrared and mass spectroscopic instruments. Results indicated differences in the exothermic values of UN thermal decomposition when compared to a dedicated DSC. The above-mentioned studies represent some of the relevant AN thermal analysis issues that arise with commonly used DSC and TGA techniques.

The data obtained with these instruments may underestimate the explosive potential of a HME material under certain conditions [7,8]. The non-standard nature of the HME chemical composition and formulation/synthesis procedures can present a formidable challenge for forensic analysis instrumentation. Thus, improved techniques are required to provide data for adequate HME forensic identification, which may not be accomplished reliably with DSC and TGA. Development of a new methodology and database of thermal and chemical signatures, along with other thermophysical properties, of HME materials is required for different compositions and ambient conditions.

### 1.3. Investigation objectives

The objective of this investigation was to determine the thermal and chemical characteristics of selected homemade explosives, using a novel measurement technique, referred to as the laser-driven thermal reactor (LDTR), and to demonstrate its capability to uniquely detect thermal-decomposition phenomena of HME materials. The technique provides temporally resolved thermal signatures (i.e., temperature versus time thermograms) of the decomposition of HMEs for a variety of operating conditions, which can uncover trends and characteristics unique to a particular chemical substance. In addition, theoretical analysis of the thermal signatures provides further quantitative information on HME properties – all of which can be used for establishing a properties database. This work has shown that the LDTR can uncover useful information regarding the thermal and chemical behavior of trace amounts of HME material at decomposition temperatures (before thermal degradation and depletion of the sample). An investigation with samples of nitromethane and ammonium nitrate was carried out under a variety of operating conditions and protocols.

## 2. Experimental arrangement

### 2.1. Brief facility description

The LDTR experimental facility and theory of analysis are described in Nazarian and Presser [9]. Some of the salient details are repeated for clarity, along with a description of the current facility modifications for these experiments. The LDTR consists of a sphere-shaped reactor mounted within a vacuum chamber, along with integrated optical, gas supply, and computer-controlled data acquisition subsystems, see Fig. 1. At the center of the reactor, the sample material rests on a thermocouple. The reactor assembly is heated from opposing sides by an infrared laser beam to achieve nearly uniform sample temperature. The vacuum chamber allows for control of the environment (e.g., gas pressure and composition) that surrounds the sample. In general, measurements are carried out at low pressure, which eliminates thermal convection within the reactor sphere, and thus conduction and radiation are the dominant modes of heat transfer. As a result, the theoretical analysis is simplified significantly, and allows one to quantify the individual

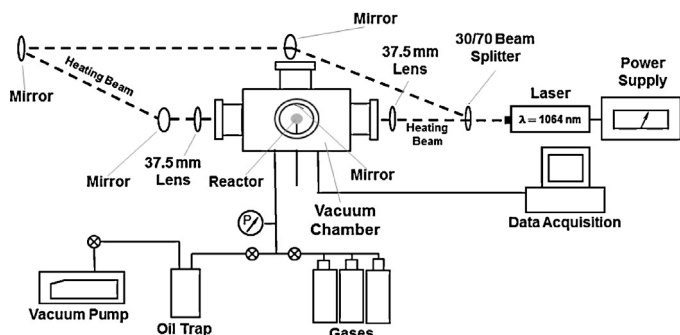


Fig. 1. Schematic of the LDTR control, optical, and gas systems.

modes of conduction and radiation heat transfer. The sample and reactor wall temperatures are recorded with respect to time by the data acquisition system and this information is then processed for the specified thermophysical and thermochemical information of interest. The mode of thermal analysis used for these experiments involves heating the reactor at two different laser fluences (referred to as the ‘heating-rate’ approach). Chemical kinetics parameters (i.e., endothermic and exothermic rate constants) of the chemical processes are also deduced from this approach.

## 2.2. Reactor design

The reactor is a small copper-foil sphere (with an outer diameter of  $18.2 \pm 0.1$  mm<sup>1</sup> and thickness of 0.14 mm) within which a sample is placed at the sphere center, see Fig. 2. The spherical reactor is fabricated by forming a thin piece of copper into a hemisphere; two pieces are then spot-welded together to form a sphere. For these experiments, a metal-spinning technique was used to improve reactor wall smoothness. The technique spin stretches the copper sheet over a precast stainless steel spherical dye. As a result of the process, the original copper material becomes thinner, which enhances the thermal conduction through the copper, decreases the heat capacity and reactor response time, and increases the heating rates (which is reduced if the foil is too thick) for the given laser power. The untreated copper foil is malleable, however, after being formed into a sphere the material is fairly rigid and does not deform easily. An opening is cut in the top of the sphere (diameter of  $\approx 7.2$  mm) to place the sample and another opening is made in the bottom (diameter of  $\approx 4.0$  mm) to introduce a four-passage ceramic tube that supports the wires and exposed beads (junctions) of two thermocouples. The reactor and substrate are placed prior to use in a small nonsmoking methanol flame under ambient conditions to generate a copper oxide, i.e., copper (II) oxide/CuO layer, which improves laser absorption and reduces beam scattering effects off of their surfaces.

## 2.3. Thermocouple design

At the center of the reactor, the sample rests on extended thermocouple wires from near the bead of one K-type fine-wire thermocouple, i.e., ‘sample’ thermocouple, see insert in Fig. 2. If needed, a disk-shaped substrate (of copper or gold-plated copper

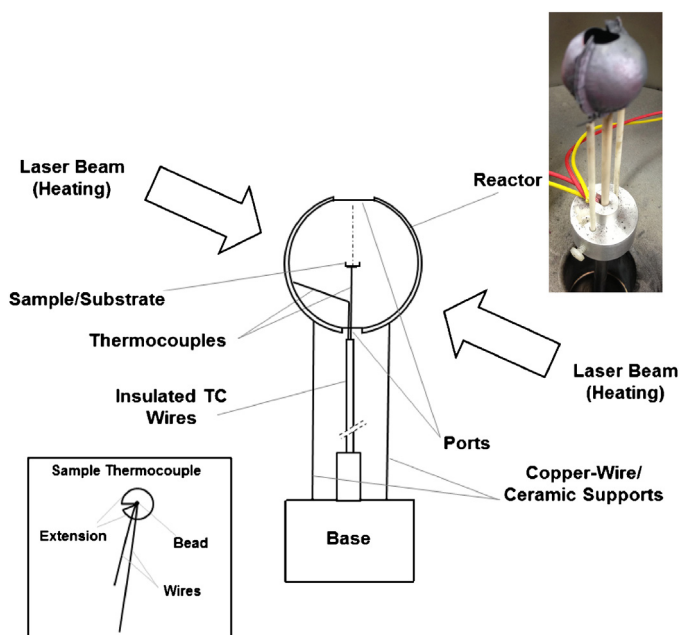


Fig. 2. Schematic of the LDTR reactor sphere. The reactor diameter is approximately 18.2 mm with an opening in the top and bottom. The insert details the sample thermocouple located in the center of the reactor.

Table 1  
Thermocouple time-response measurements.

Case	Custom thermocouple time response [s]	Thermocouple time response [s] (Omega [12])
1	0.200	
2	0.210	
3	0.200	
4	0.200	
5	0.200	
6	0.200	
7	0.198	
8	0.198	
Average	$0.200 \pm 0.002$	0.280

with a diameter of approximately 5 mm and thickness of 0.14 mm) is used to support the sample on the extensions. The wire extensions are arranged so that the thermocouple bead is in direct contact with the sample/pan. It has been demonstrated that the pan has negligible influence on the results [11]. The reactor inner wall is in contact with a second thermocouple (i.e., ‘reactor’ thermocouple), which is bent from the central ceramic tube (i.e., through the bottom port of the reactor) to the reactor inner wall surface and is flush with the wall at a vertical distance of approximately 4.5 mm from the bottom of the sphere. The thermocouples were customized in-house using spot-welding technology. The bead diameter for both thermocouples was 0.25 mm. Additionally, the sample wire bead is flattened to ensure the secure placement of the substrate. The sample thermocouple time response was calibrated using a manufacturer’s test protocol [12]<sup>2</sup> in a similar environment as that of commercially available thermocouples. The results of this calibration are given in Table 1, which shows a 40% improvement (as compared to commercial thermocouples with the same size

<sup>1</sup> Estimation of the measurement uncertainty for this study is determined from statistical analysis of a series of replicated measurements (referred to as Type A evaluation of uncertainty), and from means other than statistical analysis (referred to as Type B evaluation of uncertainty) [10]. The Type A uncertainty is calculated as  $ku_c$ , where  $k$  is the coverage factor and  $u_c$  is the combined standard uncertainty. The value for  $u_c$  is estimated statistically by  $sn^{-1/2}$ , where  $s$  is the sample standard deviation and  $n$  is the number of samples. For  $n = 50$ ,  $k = 2.01$ , representing a level of confidence of 95%.

<sup>2</sup> Certain commercial equipment or materials are identified in this publication to specify adequately the experimental procedure. Such identification does not imply recommendation or endorsement by the National Institute of Standards and Technology, nor does it imply that the materials or equipment are necessarily the best available for this purpose.

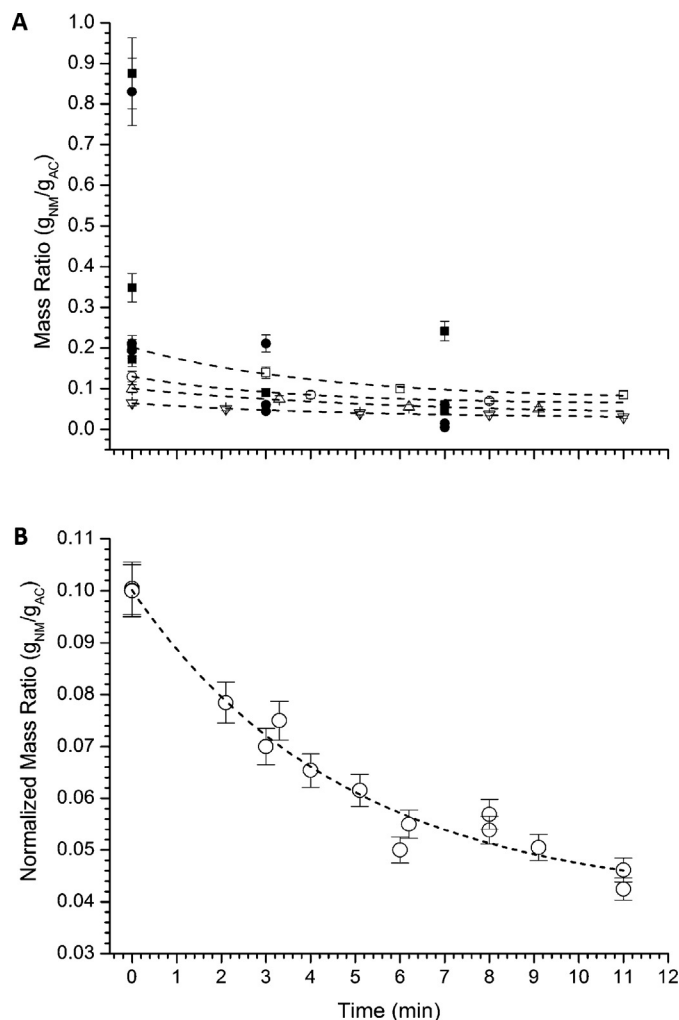


**Fig. 3.** Calibration of the nitromethane (NM) mass loss during sample preparation (with activated carbon (AC) as the substrate). A) Variation of the NM/AC mass ratio with time for different initial mass ratios. B) The NM/AC mass ratio normalized to  $Y_0 = 0.1$ .

wire) in the thermocouple time response at 63.2% of an instantaneous temperature change. The resulting sample thermocouple time response was considered sufficient for carrying out the measurements (at a data acquisition rate of three samples  $s^{-1}$ ).

#### 2.4. Heating source

The reactor is positioned near the center of a 5 L vacuum chamber with five viewing ports and a manually operated linear traverse to enable reactor accessibility (see Fig. 1). The top of the chamber provides access to the reactor and is sealed with an o-ring. Each viewing port includes a vacuum-sealed 76 mm diameter quartz window, which is suitable for transmission of laser beams to the reactor. The source of the laser beams is a 250 W multi-mode, continuous-wave Nd:YAG laser, operating at a wavelength of 1.064  $\mu\text{m}$ . Some advantages of using laser heating over other heating methods, such as electrical resistance heating, include higher heating rates, direct reactor heating to the sample to eliminate convective heating of the surrounding gases, and measurement of the total thermal loss (including both thermal and chemical contributions) with direct sample heating. The infrared laser beam heats the reactor from opposing sides using concomitant optics to direct the beam to the reactor, as shown in Figs. 1 and 2. Different temperature regimes can be interrogated by changing the laser fluence.

Substances that can be analyzed include solids, liquids, and various multiphase and multicomponent inhomogeneous substances. The laser beam is expanded with a lens to about the diameter of the sphere to reduce the temperature variation over the reactor surface [9,11]. The large thermal conductivity of the thin-walled copper sphere helps smooth out effects due to non-uniformity of the multimode laser beam intensity. The sample is heated via radiative transport from the inside surface of the reactor sphere. The high thermal conductivity of the copper sphere, and radiation heat transfer between the interior sphere surface and the sample within the sphere, was measured to provide nearly uniform sample temperature [9,11]. This uniformity in sample temperature depends on the relative dimensions of the sample and reactor sphere, laser beam width, and reactor thermal conductivity. The effects of temperature on thermal conductivity and specific heat of copper are taken into account.

Heating rates on the order of several hundred Kelvin per second can be achieved, depending on the maximum achievable laser power, sample size, and time response of the thermocouple. The apparatus can analyze sample masses from a milligram up to a few grams. The surrounding environment can handle a variety of gas compositions and pressures. In this study, nitrogen was used (supplying a nonreactive inert gas to the sample surface) at chamber gauge pressures between 1.3 and 6.7 kPa.

#### 2.5. HME precursors

The HME-precursor nitromethane is a liquid energetic material (propellant) that can be used as a fuel to mix with a solid (powdered) oxidizer like ammonium nitrate. In this investigation, nitromethane (NM) and ammonium nitrate (AN) were studied individually to isolate and characterize the individual compounds. In addition, the use of such chemicals required modification of the reactor to ensure its safe and reliable operation. The issue of possible thermocouple and reactor-material oxidation was addressed by gold-plating the inner surface of the copper reactor sphere and substrate. Also addressed were issues regarding evacuating safely the gas by-products after each experiment.

##### 2.5.1. Nitromethane

Measurements were carried out to characterize the change in nitromethane mass during the experimental preparation (see Fig. 3). The NM vapor pressure is 3.6 kPa at 20 °C and evaporation of the liquid occurs continually at ambient conditions. Nitromethane was isolated from chemically reacting with powdered oxidizer during these experiments by using a preformed piece of porous activated carbon (AC). The AC acts as an inert medium to retain the liquid and provides a large surface area (as with a powdered oxidizer). Since AC is porous, the liquid nitromethane maximizes contact surface area by filling the internal pores and coating the external surface. Experiments were performed in an inert nitrogen environment; it was confirmed that the AC did not react with the nitrogen or nitromethane by measuring its mass before and after each experiment. Nitromethane was also compared to a set of data from prior experiments to establish measurement repeatability.

##### 2.5.2. Ammonium nitrate

Ammonium nitrate of 99.8% purity was used with no further treatment or purification. The samples formed 2 mm clusters of smaller particles. The particle size was greater than 500  $\mu\text{m}$ , as measured by using an optical/digital microscope. Sample was a bulk chemical composed of irregular shaped particles. Fig. 4 presents an image of a typical AN sample consisting of 200–500  $\mu\text{m}$  size particles aggregated into 2–3 mm size clusters. For each experiment, sample was retrieved from the container and carefully placed on the substrate. The substrate mass was measured before and after

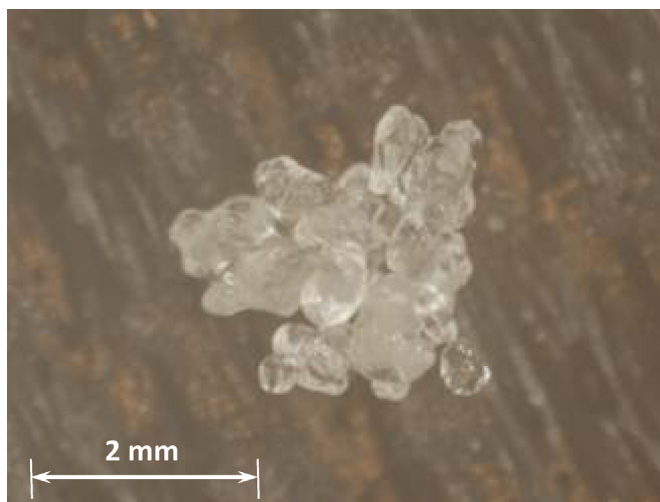


**Fig. 4.** Ammonium nitrate sample consisting of 200–500  $\mu\text{m}$  primary particles aggregated in a 2–3 mm sized cluster.

adding the AN sample. If needed, additional AN was added to the sample to achieve the targeted mass for the experiment.

Ammonium nitrate has been studied extensively in the past [4,5,7,13–19]. Most of this work has focused on understanding its thermal stability and addressing safety issues for storage and transportation of AN-based fertilizers. For explosive applications, AN has also been investigated extensively for many years. A summary of possible chemical reactions that describe the thermal decomposition of AN under various conditions is presented in Table 2 [20]. For AN heated at atmospheric pressure, thermal decomposition occurs at 230 °C and deflagration occurs at 325 °C. The boiling point of the pure material is 210 °C.

### 3. Theoretical considerations of the methodology

#### 3.1. Thermal energy balance

The theoretical model is based on a representation of the heating process associated with the above-mentioned experimental arrangement. The theoretical model is representative of samples with a small Biot number ( $<0.1$ ). In this limit, the assumption of a thermally lumped sample temperature is appropriate (i.e., no internal temperature gradients within the sample [11]). Additional details are given by Nazarian and Presser [9], and Nazarian [21]. The following thermal energy balance governs the heating process:

$$\frac{m(t)c_p(T)dT}{dt} = R_1(T_r) - R_2(T) = I_l A \beta(T, \lambda) - F(T, T_o) + \Delta m(t) q(T) \quad (1)$$

where the rate of change of sample internal thermal energy is given by the term on the left side of Eq. (1),  $R_1(T_r)$  is the rate at which heat is transferred from the reactor at temperature  $T_r$  to the sample, and  $R_2(T)$  is the rate of heat loss from the sample,  $T$  is the sample temperature,  $c_p(T)$  is the sample specific heat capacity at the sample temperature,  $m(t)$  is the sample mass with respect to time  $t$ . The first term on the right side of the Eq. (1) is the thermal energy absorbed by the sample, where  $I_l$  is the laser beam incident radiation intensity that heats the sample,  $A$  is the sample geometric cross-sectional area,  $\beta(T, \lambda)$  is the sample hemispherical absorptivity at temperature  $T$  and laser wavelength  $\lambda$ . The heat transfer term,  $F(T, T_o)$ , represents the sample thermal energy losses due to conduction, convection, and radiation throughout the arrangement. The parameter  $T_o$  is the sample temperature at steady state. Thermal energy losses due to chemical reaction and vaporization are

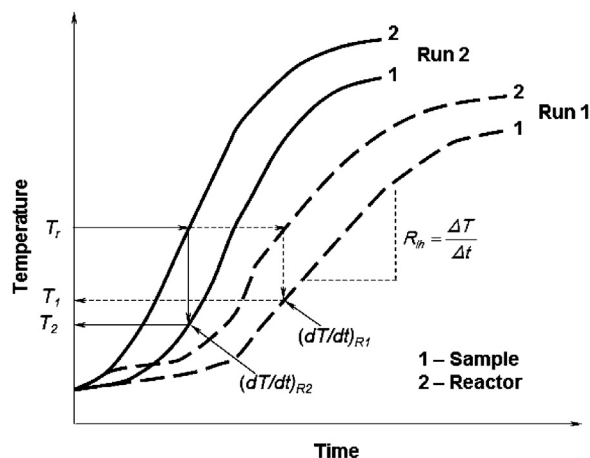


**Fig. 5.** Schematic indicating the selection of the sample temperatures for evaluating the relaxation time ( $\tau$ ) expression, given by Eq. (4).

considered if there is a detectable mass change,  $\Delta m(t)$ , after heating the sample, with  $q(T)$  defined as the specific heat release rate due to chemical reactions (i.e., the rate at which thermal energy is released or absorbed by a substance per unit mass during chemical reactions).

#### 3.2. Analysis protocol

An exponentially decaying expression for the rise in temperature of the form:

$$T - T_o = (T_a - T_o)e^{(-t/\tau)} \quad (2)$$

is assumed since it fits satisfactorily the experimental data in the regions of interest [11]. The term  $T_a$  is the ambient temperature, and  $\tau$  is the temperature-dependent relaxation time. Taking the derivative of Eq. (2) with respect to time results in the expression:

$$\frac{dT}{dt} = \frac{-(T - T_o)}{\tau} \quad (3)$$

An analytical expression is derived for  $\tau$  from Eqs. (2 and 3), which is based on obtaining the sample temperature for two different laser fluences (without the reactive sample) from a common value of the reactor temperature,  $T_r$  (see Fig. 5), and is given by:

$$\tau(T) = \frac{T_2 - T_1}{(dT/dt)_1 - (dT/dt)_2} \quad (4)$$

where  $T_1$  and  $T_2$  are the sample temperatures at time  $t$ , and  $(dT/dt)_1$  and  $(dT/dt)_2$  are the sample temperature–time derivatives (corresponding to  $T_1$  and  $T_2$ ), for the two different laser fluences, respectively. To compare the sample temperature obtained at the two different heating rates, the reactor temperature must remain unchanged. To accomplish this, a reactor temperature is chosen (with sufficient sensitivity to determine the temperature–time derivatives). Then the two sample temperatures ( $T_1$  and  $T_2$ ) and corresponding sample temperature–time derivatives are obtained by extrapolation to the appropriate curves, as illustrated in Fig. 5. The value of  $\tau$  is determined from Eq. (4) without the sample (i.e., with only the AC substrate) and thus it is assumed that the thermal energy balance equation for the sample (see Eq. (1)) is the sum of a nonreacting and chemical reacting expression, and that the difference in thermograms between the two experiments (i.e., with and without sample) will be similar. This value of  $\tau$  will remain unchanged for a particular sample and sample temperature. It can be shown that the inverse of the relaxation time with respect to the sample temperature is a linear relationship, as shown in Fig. 6 for

**Table 2**  
Ammonium nitrate decomposition reactions [20].

No.	Reaction	Comments
1	$\text{NH}_4\text{NO}_3 \rightarrow \text{HNO}_3 + \text{NH}_3$	This reaction occurs at a temperature above the melting point of ammonium nitrate
2	$\text{NH}_4\text{NO}_3 \rightarrow \text{N}_2\text{O} + 2\text{H}_2\text{O}$	This reaction occurs in the temperature range of 180–200 °C when ammonium nitrate is unconfined. Oxides other than $\text{N}_2\text{O}$ form at 203–285 °C
3	$\text{NH}_4\text{NO}_3 \rightarrow \text{H}_2 + 1/2\text{O}_2 + \text{H}_2\text{O}$	This reaction occurs when ammonium nitrate is heated under strong confinement or when initiated by a detonation
4	$\text{NH}_4\text{NO}_3 \rightarrow \text{NO} + 1/2\text{N}_2 + 2\text{H}_2\text{O}$	This reaction occurs during incomplete detonation (at a pressure of 4860 kg $\text{cm}^{-2}$ and temperature of approximately 518 °C)
5	$\text{NH}_4\text{NO}_3 \rightarrow 1/2\text{H}_2\text{N}_2 + 3/4\text{NO}_2 + 1/4\text{NO} + 1/4\text{N}_2 + 5/4\text{H}_2\text{O}$	Decomposition reaction that occurs when ammonium nitrate is under confinement at 200–260 °C. This endothermic reaction is followed (at 260–300 °C) by an explosion of the gaseous reaction products
6	$3\text{NH}_4\text{NO}_3 \rightarrow 2\text{N}_2 + \text{N}_2\text{O}_3 + 6\text{H}_2\text{O}$	This reaction cannot take place alone because $\text{N}_2\text{O}_3$ exists only in the dissociated state as $\text{NO} + \text{NO}_2$
7	$4\text{NH}_4\text{NO}_3 \rightarrow 2\text{NO}_2 + 3\text{N}_2 + 8\text{H}_2\text{O}$	This reaction occurs during incomplete detonation
8	$4\text{NH}_4\text{NO}_3 \rightarrow 3\text{NO}_2 + 5\text{H}_2\text{O} + \text{N}_2 + \text{NH}_3 + \text{NO}$	This reaction is similar to the endothermic reaction (7). If the gaseous reaction products are heated, an explosive exothermic reaction takes place
9	$5\text{NH}_4\text{NO}_3 \rightarrow 2\text{HNO}_3 + 4\text{N}_2 + 9\text{H}_2\text{O}$	This reaction occurs under certain conditions such as in the presence of spongy platinum and gaseous $\text{HNO}_3$
10	$8\text{NH}_4\text{NO}_3 \rightarrow 16\text{H}_2\text{O} + 2\text{NO}_2 + 5\text{N}_2$	This reaction occurs during incomplete detonation

The values for the heat liberated are at ambient pressure and temperature (18 °C) for solid ammonium nitrate with all decomposition products in gaseous form. None of these reactions occur as a single reaction, but are always accompanied by other reactions. The predominate reactions are: Reaction Nos. 2, 7, and 8.

nitromethane and ammonium nitrate. The data for both samples agree to within 15% of the linear fit. One can then interpolate from Fig. 6 values of  $[\tau]^{-1}$  for different measured sample temperatures.

Once the relaxation time is known, separate experiments can be carried out at a particular laser fluence, i.e., one with only the AC substrate (baseline), and a second with the sample (either NM or AN) and substrate. The equations representing these two experiments are:

With both the sample and substrate

$$\frac{m(t)c_p(T)dT}{dt} = I_l A \beta(T, \lambda) - F(T, T_o) + \Delta m(t)q(T) \quad (5)$$

Without the sample (substrate only)

$$\frac{m(t)c_p(T)dT}{dt} = I_l A \beta(T, \lambda) - F(T, T_o) \quad (6)$$

We assume that  $m_{sas} \approx m_{so} \equiv m$ ,  $c_{p,sas} \approx c_{p,so} \equiv c_p$ , and  $\beta_{sas} \approx \beta_{so} \equiv \beta$  (where the subscript 'sas' refers to the combined sample and substrate in Eq. (5) and the subscript 'so' refers to the substrate only in Eq. (6)) since the mass of the sample is small compared to the substrate mass. Subtracting Eq. (6) from Eq. (5),

substituting into Eq. (4), and rearranging terms results in the following expression for the specific heat release rate,  $q(T)$ , due to chemical reaction:

$$q(T_{sas}) = \frac{c_p(T_{sas})m(t)}{\Delta m(t)} \left[ \frac{T_{sas} - T_{so}}{\tau} + \left. \frac{dT}{dt} \right|_{sas} - \left. \frac{dT}{dt} \right|_{so} \right] \quad (7)$$

where one can estimate all of the terms to determine the value of  $q(T)$ . Note that Eq. (7) is independent of the laser beam incident radiation intensity. Integration of Eq. (7) with respect to time (for the entire experiment, which includes the combination of endothermic and exothermic processes) results in an expression for the total specific heat release,  $Q = \int q(T) dt$ , which in turn is equal to  $-\Delta H$  (where  $\Delta H$  is the change in enthalpy of a chemical reaction) [9]. One can then compare the measured change in enthalpy to calculated values, which are derived from the set of possible overall chemical reactions (i.e., as obtained from the literature). The most probable reaction is assumed to be the one with a calculated value of  $\Delta H$  that is similar to the measured value.

### 3.3. Thermogram correction

As described earlier, the LDTR methodology relies on comparison of two data sets of time-dependent temperature profiles (thermograms), i.e., each set includes a reactor and sample temperatures thermogram. One set is with the reactive sample (for which endothermic/exothermic processes occur) and the second is a baseline measurement (i.e. without sample). For each set, initiation of the laser heating may be different during data acquisition of the temperature readings. To address this issue, the reactor temperatures profiles should be similar because the laser fluence is the same for both the sample and baseline runs. Thus, an adjustment of the starting point on the time (abscissa) scale of one dataset is carried out so that the two reactor-temperature thermograms overlay one another. This then allows for comparison and analysis of the two sample-temperature thermograms, i.e., with and without (baseline) the reactive material. Further analysis of the thermograms to extract the specific heat release rate during selected portions of the heating process is detailed by Nazarian and Presser [9].

## 4. Results and discussion

Homemade explosives are often composed of mixtures of both solid oxidizer (e.g., AN) and liquid fuel (e.g., NM). The oxidation of the fuel is heterogeneous, and the rate of reaction will depend on the contact surface area between the fuel and oxidizer. It is

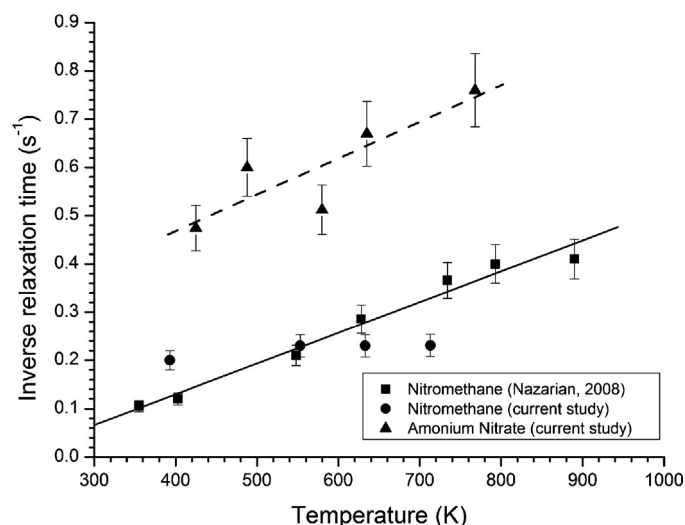


**Fig. 6.** Variation of inverse relaxation time with sample temperature for nitromethane (NM) and ammonium nitrate (AN). Linear data regression results in following relationships:  $[\tau]^{-1} = -0.075 + 0.163 (T [K]/300) [s^{-1}]$  for NM, and  $[\tau]^{-1} = -0.166 + 0.227 (T [K]/300) [s^{-1}]$  for AN.

documented (e.g., [22]) that extremists often grind porous solids into powders to increase surface area and improve the total exothermic energy release. Porous surfaces can be thought of being composed of an internal surface (i.e., network of pores) and external outer surface. The large internal solid surface absorbs, retains, and augments the oxidizer contact area with the liquid fuel to exploit chemical reactions. Vaporization and dripping occur more readily on the external surface. Thus, oxidizer porosity and particle size are critical parameters for HME explosive applications.

To this end, experiments were carried out to study the thermal decomposition of nitromethane and ammonium nitrate. In general, nitromethane is an additive to ammonium nitrate; however, results for isolated nitromethane and ammonium nitrate will be important for evaluating the thermal degradation of such mixtures in the future. The thermal energy release and chemical kinetics information were obtained for both substances at different temperatures, sample masses, and heating rates. Analyses were carried out to identify substance thermal behavior, i.e., exothermic and endothermic processes. The endothermic behavior is assumed to be attributed to organics (if present), water vaporization, melting, solid phase transition, and/or chemical/thermal decomposition, while exothermic behavior is attributed to the occurrence of chemical reactions and possibly the presence of accelerated rates of thermal energy release (which may be indicative of uncontrolled reaction rates due to the energetic nature of the material).

#### 4.1. Change in nitromethane mass during the experiment preparation

As mentioned earlier, the specific heat release rate is determined at different stages of reaction (i.e., endothermic or exothermic) and the total specific heat release is compared to literature values of the change in enthalpy for the various possible chemical reactions. Since activated carbon is a porous material, the heterogeneity of the liquid NM as it wets the AC surface will influence its vaporization after sample preparation, and consequently its mass and determination of the specific heat release rate. Care was therefore taken to account for the changes in mass during preparation of the sample and experimental condition (i.e., sample vaporization increases while under vacuum), and during the initial heating of the sample (i.e., detection of an endothermic phase in the thermograms). Fig. 3 presents the mass ratio of nitromethane to activated carbon with respect to time, with the data at time  $t = 0$  representing an initial sample mass ratio. Sample was placed in the reactor and the experiment prepared to the point prior to laser heating (i.e., under vacuum). The sample was then removed, reweighed and the time noted.

The data were normalized to obtain an empirical mathematical expression that was based on the initial NM/AC mass ratio and sample preparation time (i.e., time from coating the activated carbon with nitromethane to the moment prior to laser heating of the sample within the vacuum chamber). The variation of the NM/AC mass ratio with time was determined for different initial NM/AC mass ratios (see Fig. 3A). Three AC samples were prepared with sample sizes of 22.9, 31.2, and 55.1 mg. The nitromethane liquid was gradually added to the AC using a pipette and then reweighed. Each of the three NM/AC samples was placed in the vacuum chamber, and the air gradually evacuated to a vacuum pressure of about 1.3 kPa. Vacuum pressures of less than 6.7 kPa are generally used to ensure negligible convective heat transfer during experiments. After remaining in the vacuum chamber for different lengths of time, each sample was retrieved and the mass re-measured. The results are normalized to  $Y_0 = 0.1$  where  $Y_0$  is the initially prepared NM/AC mass ratio, and are presented in Fig. 3B. The resulting curve fit to the data is  $Y = Y_0 (0.4 + 0.6e^{-t/4.78})$  where  $Y$  is the NM/AC mass

ratio, and  $t$  is the change in time between the initial and final sample mass readings.

The resulting figure is a calibration curve for the evaporation rate of nitromethane, but more so the results indicate that when liquid is coating the external surface (for an initial NM/AC mass ratio of about  $0.3 \text{ g}_{\text{NM}} \text{ g}_{\text{AC}}^{-1}$ ), the rate of vaporization increases. This is attributed to the liquid on the external surface evaporating more readily than the liquid within the activated carbon pores. Thus, keeping the mass ratio such that there is little liquid coating the external surface can provide consistent results and a more precise assessment of the initial nitromethane mass when initiating laser heating. One can then obtain the sample mass change by extracting and weighing the sample after completion of the experiment. With a more precise estimate of the initial and final sample mass, evaluation of the thermograms then enabled quantification of the total exothermic energy release for nitromethane decomposition. The measured change in enthalpy was determined and compared with the calculated change in enthalpies from chemical reactions available in the literature, as given in Table 3. Three out of seven possible reactions (Reactions 3, 4, and 5) in Table 3 are considered likely candidate reactions taking part in the chemical degradation of nitromethane, since the calculated change in enthalpies compares well with the measured value.

#### 4.2. Effect of sample mass and laser heating rate on ammonium nitrate decomposition

Experiments with ammonium nitrate were conducted to evaluate the measurement sensitivity of the thermal response (i.e., the endothermic and exothermic nature of the reactions), and other thermogram features (e.g., melting point), which might provide useful information for forensic thermal analysis. The effect of the initial sample mass and laser heating rate on the AN thermal behavior were evaluated with all other experimental parameters remaining unchanged. Measurements with AN were carried out for following conditions: pressures of  $4.7 \pm 2.0$  kPa in nitrogen for different sample masses ranging between  $2.3 \pm 0.1$  and  $8.0 \pm 0.1$  mg, and heating rates ( $R_{lh}$ ) of 30, 47, 60, 80, and  $85 \text{ K s}^{-1}$ . The values for  $R_{lh}$  were derived by determining the slope of the near-linear temperature-rise portion of the baseline thermogram (see Fig. 5) for different laser power control settings. A power meter was not used to distinguish between the settings because of the uncertainty in knowing how much of the beam intensity actually impacts the sample. The measurement uncertainty was estimated to be less than 10% of the stated values. Different segments of the thermograms were identified as being endothermic or exothermic by comparing the sample temperatures to the baseline (i.e., without AN) thermogram. Results for the temperature difference and temperature-time derivative with respect to time were analyzed to enhance the measurement sensitivity of the small temperature changes that are associated with the thermograms. The measured change in enthalpy was also compared to values (from corresponding chemical reactions) found in the literature.

To demonstrate the measurement responsiveness to laser heating rate and its importance for characterizing substance decomposition, Fig. 7 (taken from Nazarian and Presser [9]) presents the temperature difference (between the sample and reactor temperatures) with respect to time, using activated carbon pellets at three different heating rates. In this case, the AC consisted of two major components (i.e., carbon and organic volatile matter) and the experiment was carried out in an oxidizing environment (i.e., air). For a heating rate of  $3 \text{ K s}^{-1}$  and an operating temperature of about 400 K, the results indicate the presence of two peaks that form preferentially with time. The earlier peak is attributed to the thermal decomposition of the volatile matter and the later peak is attributed to the thermal decomposition (i.e., combustion) of the carbon. Both

**Table 3**

Calculated and measured change in enthalpy (or negative value of the total specific heat release) for all known nitromethane chemical reactions during thermal decomposition [26].

No.	Reaction	Calculated change in enthalpy [kJ g <sup>-1</sup> ]	Measurement change in enthalpy [kJ g <sup>-1</sup> ]
1	$\text{CH}_3\text{NO}_2(\text{l}) \rightarrow \text{CO}_2(\text{g}) + 3/2\text{H}_2(\text{g}) + 1/2\text{N}_2(\text{g})$	4.602	$5.3 \pm 0.5$
2	$\text{CH}_3\text{NO}_2(\text{l}) \rightarrow \text{CO}(\text{g}) + \text{H}_2\text{O}(\text{g}) + 1/2\text{H}_2(\text{g}) + 1/2\text{N}_2(\text{g})$	3.927	
3	$\text{CH}_3\text{NO}_2(\text{l}) \rightarrow 1/4\text{CO}_2(\text{g}) + 3/4\text{C}(\text{g}) + 3/2\text{H}_2\text{O}(\text{g}) + 1/2\text{N}_2(\text{g})$	5.709	
4	$\text{CH}_3\text{NO}_2(\text{l}) \rightarrow 1/2\text{CO}(\text{g}) + 1/2\text{C}(\text{g}) + 3/2\text{H}_2\text{O}(\text{g}) + 1/2\text{N}_2(\text{g})$	5.002	
5	$\text{CH}_3\text{NO}_2(\text{l}) \rightarrow 5/8\text{CO}_2(\text{g}) + 3/4\text{H}_2\text{O}(\text{g}) + 3/8\text{CH}_4(\text{g}) + 1/2\text{N}_2(\text{g})$	5.614	
6	$\text{CH}_3\text{NO}_2(\text{l}) + 7/4\text{C}(\text{g}) \rightarrow 2\text{CO}(\text{g}) + 3/4\text{CH}_4(\text{g}) + 1/2\text{N}_2(\text{g})$	2.692	
7	$\text{CH}_3\text{NO}_2(\text{l}) + 2\text{C}(\text{g}) \rightarrow 1/2\text{C}_2\text{H}_6(\text{g}) + 2\text{CO}(\text{g}) + 1/2\text{N}_2(\text{g})$	2.464	

are exothermic processes yet triggered at different threshold temperatures. Although not examined, the DSC would not be expected to resolve the earlier peak at the given operating temperature because of the relatively low DSC heating rate. At a higher heating rate of  $15 \text{ K s}^{-1}$  and operating temperature of about 600 K, essentially one peak forms, and is attributed to thermal decomposition of all volatile matter and the immediate transition to combustion of the carbon. This result demonstrates how the heating rate can be adjusted (optimized) based on the composition of an HME to reveal different thermal and chemical reaction phenomena.

A dependency of ammonium nitrate thermal behavior was found for both increasing heating rate (see Fig. 8) and sample mass (see Fig. 9). Fig. 8 presents the sample temperature–time derivative with respect to sample temperature (Fig. 8A) and time (Fig. 8B) for different heating rates of 30, 47, 60, 80,  $85 \text{ K s}^{-1}$ . Each curve represents an independent experiment for measurements carried out at the same conditions (i.e., in nitrogen at a pressure of 6.7 kPa and for a sample mass of  $2.3 \pm 0.1 \text{ mg}$ ). A change in the derivative as temperature increased was found for  $R_{lh} = 47, 60, 80,$  and  $85 \text{ K s}^{-1}$ , but not for  $R_{lh} = 30 \text{ K s}^{-1}$ . This result indicates that there is some transition in the manifestation of chemical reactions, which occurs between  $R_{lh} = 30 \text{ K s}^{-1}$  and  $R_{lh} = 47 \text{ K s}^{-1}$ , and does not change further for the higher heating rates.

A similar feature was found for the change in sample mass at constant operating conditions; see the sample temperature–time derivative with respect to sample temperature in Fig. 9A and time in Fig. 9B. Each curve again represented an independent experiment. The operating conditions were for a nitrogen environment at a pressure of 6.7 kPa and heating rate of  $30 \text{ K s}^{-1}$ . The different

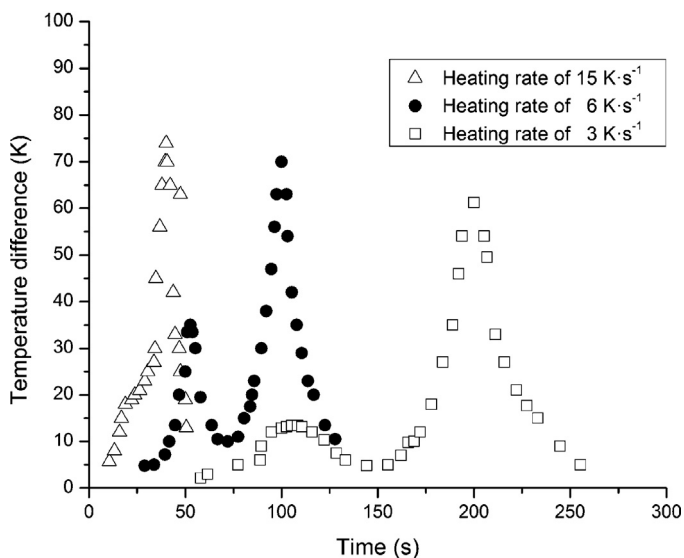


**Fig. 7.** Variation of the difference in temperature between the reactor and sample with time for activated carbon pellets at three different laser heating rates ( $R_{lh}$ ).

sample masses were 2.3, 3.5, and  $8.0 \pm 0.1 \text{ mg}$ . For this case, the results indicate that there is some transition in the occurrence of chemical reactions, which occurs between a sample mass of  $2.3 \pm 0.1$  and  $3.5 \pm 0.1 \text{ mg}$ , and does not change further for the larger mass.

Fig. 10 presents a typical ammonium nitrate thermal signature from the LDTR and a conventional differential thermal analyzer (DTA) [23,24]. The LDTR heating rate was about 200 times faster than that of the DTA, which resulted in a much stronger signal with respect to time. The LDTR result also denoted clearly important thermal-related features for ammonium nitrate, such as the

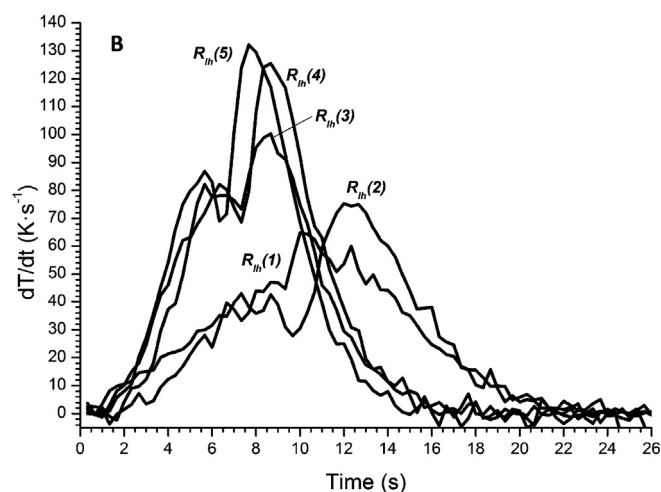
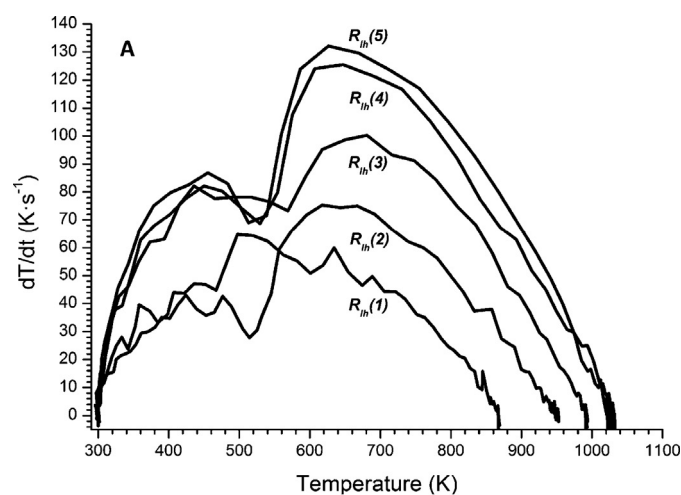


**Fig. 8.** Variation of the temperature–time derivative ( $dT/dt$ ) with A) sample temperature, and B) time, for ammonium nitrate, different laser heating rates ( $R_{lh}$ ), and a sample mass of  $2.3 \pm 0.1 \text{ mg}$ .  $R_{lh}$  (1) =  $30 \text{ K s}^{-1}$ ,  $R_{lh}$  (2) =  $47 \text{ K s}^{-1}$ ,  $R_{lh}$  (3) =  $60 \text{ K s}^{-1}$ ,  $R_{lh}$  (4) =  $80 \text{ K s}^{-1}$ ,  $R_{lh}$  (5) =  $85 \text{ K s}^{-1}$ .

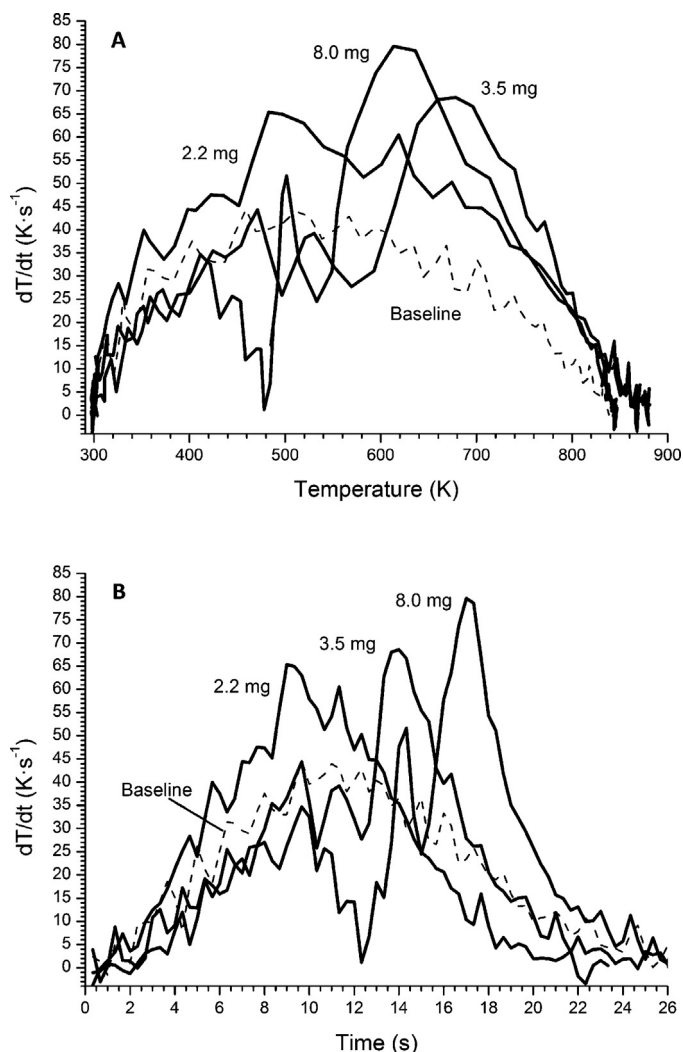


**Fig. 9.** Variation of the temperature–time derivative ( $dT/dt$ ) with A) sample temperature, and B) time, for ammonium nitrate, different sample masses and a laser heating rate ( $R_{lh}$ ) of  $30 \text{ K s}^{-1}$ . Baseline represents experiment without ammonium nitrate (substrate only).

melting, boiling, and thermal-decomposition temperatures (see the table in Fig. 10). Furthermore, the slower heating rate of the commercial instrument resulted in depletion of the sample (due to boiling and evaporation) before reaching the threshold temperature of the exothermic process.

The value of the measured change in enthalpy is important for providing a better understanding of the overall chemical reaction of an HME explosive blast, and defining mitigation strategies. Table 4 presents the calculated change in enthalpy for various possible reactions of ammonium nitrate, and Table 5 presents the

**Table 4**

Calculated change in enthalpy for all known ammonium nitrate chemical reactions during thermal decomposition.

No.	Reaction	Calculated change in enthalpy [ $\text{kJ g}^{-1}$ ]	Reference/Comment
1	$2\text{NH}_4\text{NO}_3(\text{s}) \rightarrow 4\text{H}_2\text{O}(\text{g}) + 2\text{N}_2(\text{g}) + \text{O}_2(\text{g})$	1.474	Standard state (298.15 K)*
2	$\text{NH}_4\text{NO}_3(\text{s}) \rightarrow 2\text{H}_2\text{O}(\text{g}) + \text{N}_2\text{O}(\text{g})$	0.455	Standard state (298.15 K)*
3a	$\text{NH}_4\text{NO}_3(\text{s}) + 2\text{CH}_3\text{NO}_2(\text{l}) \rightarrow 5\text{H}_2\text{O}(\text{g}) + 2\text{N}_2(\text{g}) + 2\text{CO}(\text{g})$	10.5	Standard state (298.15 K)*
3b	$\text{NH}_4\text{NO}_3(\text{s}) + 2\text{CH}_3\text{NO}_2(\text{g}) \rightarrow 5\text{H}_2\text{O}(\text{g}) + 2\text{N}_2(\text{g}) + 2\text{CO}(\text{g})$	11.3	Standard state (298.15 K)*
4	$\text{NH}_4\text{NO}_3(\text{s}) \rightarrow \text{NH}_3(\text{g}) + \text{HNO}_3(\text{g})$	2.120	Standard state (298.15 K)*
5	$\text{NH}_4\text{NO}_3(\text{s}) \rightarrow \text{NH}_4\text{NO}_3(\text{g})$	-1.687	Standard state (298.15 K)**
6	$\text{NH}_4\text{NO}_3(\text{s}) \rightarrow 2\text{H}_2\text{O}(\text{g}) + \text{N}_2(\text{g}) + \text{O}(\text{g})$	1.639	Akhavan [3]

\* Lide [26].

\*\* Irikura [27].

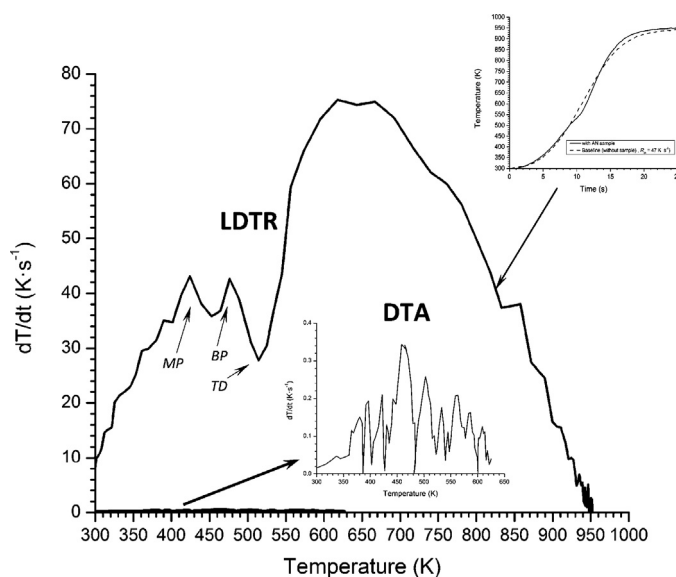


**Fig. 10.** A typical ammonium nitrate (AN) thermal signature from the LDTR and a conventional differential thermal-analysis (DTA) technique [23,24]. The LDTR insert is an example of a thermal signature, which compares the baseline (without sample) measurement with that of the AN sample for  $R_{lh} = 47 \text{ K s}^{-1}$ .

AN Thermal Properties [20]	Temperature [K]	Reaction Type
Phase Transition (PT)	357–398	Endothermic
Melting point (MP)	443	Endothermic
Boiling point (BP)	483	Endothermic
Thermal Decomposition (TD)	503	Exothermic
Deflagration (D)	598	Exothermic

AN total specific heat release measured at different laser heating rates. The calculation of the total specific heat release was obtained by dividing by the initial total mass, with corrections for the mass loss during the endothermic portion of the thermal decomposition process. Vaporization-energy data from Linstrom [25] were used to assess the effect of vaporization on the sample mass. The results indicate that for the given sample mass there is no change in the value of  $\Delta H$  with respect to the laser heating rate. This may be attributed to the fact that the dominant chemical reaction during thermal decomposition is Reaction 4 (see Table 4), and is consistent with the data presented in Table 2 [20]. Table 4 also presents values for the change in enthalpy of an AN/NM mixture (Reactions 3a and 3b), as opposed to the other reactions listed in Table 4 for AN alone. It is noted that this value is about five times larger than the other AN reactions, indicating that the behavior of the AN/NM mixture is significantly different than for AN (and NM) alone.

Fig. 11 presents the total specific heat release for the thermal decomposition of ammonium nitrate at different laser heating rates and sample sizes. Experiments were performed using two substrates, i.e., uncoated and gold-plated copper. By using two different materials, it was possible to assess the presence of chemical interaction between sample and substrate. The results indicate no

**Table 5**  
Measured change in enthalpy (or negative value of the total specific heat release) for ammonium nitrate at different laser heating rates.

Case	Sample mass [mg]	Laser heating rate [ $\text{K s}^{-1}$ ]	Measured change in enthalpy [ $\text{kJ g}^{-1}$ ]	Substrate material
1	$3.5 \pm 0.1$	30	1.41	Copper
2	$2.2 \pm 0.1$	40	2.3	Copper
3	$8.0 \pm 0.1$	20	1.89	Copper
4	$2.3 \pm 0.1$	30	2.56	Copper
5	$2.2 \pm 0.1$	60	1.86	Copper
6	$2.2 \pm 0.1$	80	2.35	Copper
7	$2.4 \pm 0.1$	85	2.17	Copper
8	$2.2 \pm 0.1$	47	2.30	Copper
9	$1.9 \pm 0.1$	33	2.16	Gold-plated
10	$1.3 \pm 0.1$	35	2.03	Gold-plated
11	$2.0 \pm 0.1$	75	2.11	Gold-plated
Average			$2.10 \pm 0.22$	

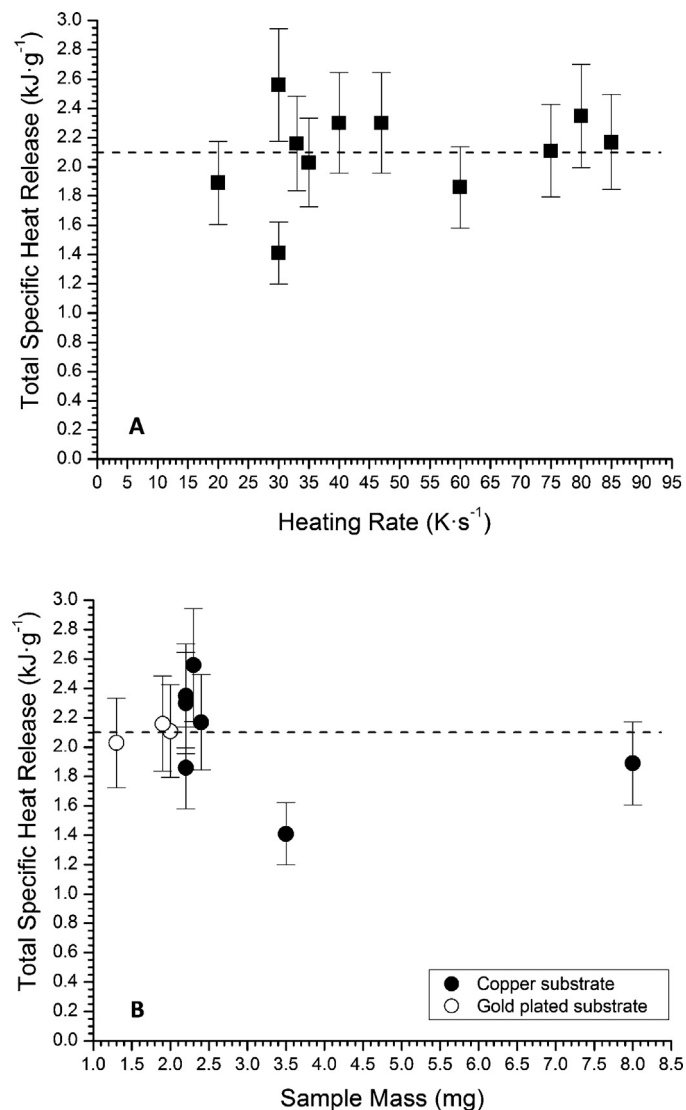


**Fig. 11.** Variation of the total specific heat release ( $Q$ ) from ammonium nitrate due to thermal decomposition for different (A) laser heating rates ( $R_{lh}$ ) and (B) sample masses (for two substrates).

significant contribution of the substrate to the release of thermal energy.

## 5. Conclusion

The laser-driven thermal reactor was shown to be an important diagnostic tool for characterizing the thermal and chemical

behavior of trace amounts of HME material at decomposition temperatures (before thermal degradation and depletion of the sample). Results indicate that the type of mixing (i.e., internally or externally) of liquid HMEs (i.e., nitromethane) with a porous material (or powder) may affect measurement repeatability. The liquid-fuel saturation of the solid internal pores appears to be a limiting parameter for the total specific heat release during exothermic processes. The contribution of the external-surface liquid fuel to the total specific heat release is negligible during thermal oxidation and vaporization due to the relatively quick liquid mass change. For this study, the threshold (i.e., when the internal surface is essentially saturated) occurs for a value of the NM/AC mass ratio at about 30%. This threshold will change depending on the physical properties (e.g., internal surface area) of the solid oxidizer. Results indicate a dependency of sample mass and laser heating rate on the thermal signatures of ammonium nitrate, which was undetectable by other commercially available thermal analysis techniques (e.g., DSC and TGA). Further development of the experimental arrangement, analysis protocol, and theoretical analysis for HME substances can ultimately result in an important measurement capability and reference database for the HME forensics community.

## Acknowledgments

This work was supported, in part, by the NIST Office of Law Enforcement Standards and the NIST Chemical Science Division. The authors would like to thank Dr. K. Yeager (FBI Lab) for the technical discussions.

## References

- [1] The White House, Policy Statement for Countering Improvised Explosive Devices, Washington, DC, 2013, [www.whitehouse.gov/sites/default/files/docs/cied.1.pdf](http://www.whitehouse.gov/sites/default/files/docs/cied.1.pdf).
- [2] Department of Defense, Joint Improvised Explosives Device Defeat Organization (JIEDDO) Broad Agency Announcement (BAA), 12-01-HME, 2011, [https://bids.acqcenter.com/JIEDDO/Portal.nsf/2BEBE7D0C82CF61E8525772B004F4F34/\\$FILE/SDA0901.pdf](https://bids.acqcenter.com/JIEDDO/Portal.nsf/2BEBE7D0C82CF61E8525772B004F4F34/$FILE/SDA0901.pdf).
- [3] J. Akhavan, *The Chemistry of Explosives*, second ed., The Royal Society of Chemistry, Cambridge, 2004, pp. 77–82.
- [4] S. Vyazovkin, J.S. Clawson, C.A. Wight, Thermal dissociation kinetics of solid and liquid ammonium nitrate, *Chem. Mater.* 13 (2001) 960–966.
- [5] J.C. Oxley, J.L. Smith, E. Rogers, M. Yu, Ammonium nitrate: thermal stability and exclusivity modifiers, *Thermochim. Acta* 384 (2002) 23–45.
- [6] S.J. Desilets, P. Brousseau, D. Chamberland, S. Singh, H. Feng, R. Turcotte, K. Armstrong, J. Anderson, Thermal decomposition of urea nitrate (UN) at higher temperatures, *Thermochim. Acta* 521 (2011) 59–65.
- [7] T.J. Janssen (Ed.), *Explosive Materials Classification: Composition and Properties*, Nova Science, 2011, pp. 125–144.
- [8] R.J. Lewis (Ed.), *Hawley's Condensed Chemical Dictionary*, Wiley, New York, 1993, p. 1063.

- [9] A. Nazarian, C. Presser, Thermal and chemical kinetic characterization of multi-phase and multicomponent substances by laser heating, *Int. J. Heat Mass Transf.* 51 (2008) 1365–1378.
- [10] B.N. Taylor, C.E. Kuyatt, Guidelines for Evaluating and Expressing the Uncertainty of NIST Measurement Results, NIST Technical Note 1297, National Institute of Standards and Technology, Gaithersburg, MD, 1994.
- [11] C. Presser, Absorption coefficient measurements of particle-laden filters using laser heating: validation with nigrosin, *J. Quant. Spectrosc. Radiat. Transf.* 113 (2012) 607–623.
- [12] Omega, Comparison of Time Constant vs. Overall Outside Diameter of Bare Thermocouple Wires or Grounded Junction Thermocouples in Air, Omega Catalogue, 2011, pp. Z-51, <http://www.omega.com/temperature/Z/pdf/z051.pdf>
- [13] S. Sreedhar, S.V. Rao, P.P. Kiran, S.P. Tewari, G.M. Kumar, Stoichiometric analysis of ammonium nitrate and ammonium perchlorate with nanosecond laser induced breakdown spectroscopy, *Proc. SPIE* 7665 (2010) 1–11, <http://acrhem.com/download/51.pdf>.
- [14] X. Zhixiang, L. Dabin, Y. Zhiwen, W. Yanan, Influence of iron ion on thermal behavior of ammonium nitrate and emulsion explosives, *Cent. Eur. J. Energetic Mater.* 7 (2010) 77–93.
- [15] K. Shah, Ammonium Nitrate Production, Storage and Distribution: Accidents and Investigations, Vol. 629, *Proc. Int'l Fertilizer Soc.*, London, 2008.
- [16] S. Kimura, H. Hata, T. Hiroe, K. Fujiwara, H. Kusano, Analysis of explosion combustion phenomenon with ammonium nitrate, *Mater. Sci. Forum* 566 (2008) 213–218, <http://www.scientific.net/MSF.566.213>.
- [17] G. Marlair, M.-A. Kordek, Safety and security issues relating to low capacity storage of AN-based fertilizers, *J. Hazard. Mater.* 123 (2005) 13–28.
- [18] N. Dechy, T. Bourdeaux, N. Ayrault, M.-A. Kordek, J.-C. Le Coze, First lessons of the Toulouse ammonium nitrate disaster, 21st September 2001, AZF plant, France, *J. Hazard. Mater.* 111 (2004) 131–138.
- [19] P.N. Simões, L.M. Pedroso, A.A. Portugal, J.L. Campos, Study of the decomposition of phase stabilized ammonium nitrate (PSAN) by simultaneous thermal analysis: determination of kinetic parameters, *Thermochim. Acta* 319 (1998) 55–65.
- [20] Department of the Army, Military Explosives, DoA Technical Manual TM 9-1300-214, 1984, <http://www.everyspec.com>
- [21] A. Nazarian, in: T.M. Gilliam, C.W. Carlton (Eds.), *Laser Driven Thermal Reactor for Hazardous Waste Stabilization, Stabilization and Solidification of Hazardous, Radioactive and Mixed Wastes*, Vol. 3, ASTM STP 1240, 1995, pp. 634–647.
- [22] J.I. Rostberg, Common Chemicals as Precursors of Improvised Explosive Devices: The Challenges of Controlling Domestic Terrorism, Naval Postgraduate School Monterey, CA, 2005, <http://www.dtic.mil/cgi-bin/GetTRDoc?AD=ADA439597>.
- [23] H. Kiiski, Stabilization of Ammonium Nitrate and AN-Based Fertilizers, *Proc. Int'l Fertilizer Soc.*, 2006, Proceedings 583.
- [24] H. Kiiski, Properties of Ammonium Nitrate-Based Fertilisers, Department of Chemistry, University of Helsinki, 2009, PhD Dissertation, [www.doria.fi/bitstream/handle/10024/47167/property.pdf](http://www.doria.fi/bitstream/handle/10024/47167/property.pdf).
- [25] P.J. Linstrom, NIST Chemistry WebBook, NIST Standard Reference Database Number 69, 2012, <http://webbook.nist.gov/chemistry/>.
- [26] D.R. Lide (Ed.), *Handbook of Chemistry and Physics*, ninety-second ed., CRC, Taylor and Francis Group, Florida, 2012.
- [27] K.K. Irikura, Thermochemistry of ammonium nitrate,  $\text{NH}_4\text{NO}_3$  in the gas phase, *J. Phys. Chem. A* 114 (2010) 11651–11653.